AMSR-E/Aqua Daily L3 25 km Brightness Temperature & Sea Ice Concentration Polar Grids, Version 3

USER GUIDE

How to Cite These Data

As a condition of using these data, you must include a citation:

Cavalieri, D. J., T. Markus, and J. C. Comiso. 2014. *AMSR-E/Aqua Daily L3 25 km Brightness Temperature & Sea Ice Concentration Polar Grids, Version 3*. [Indicate subset used]. Boulder, Colorado USA. NASA National Snow and Ice Data Center Distributed Active Archive Center. https://doi.org/10.5067/AMSR-E/AE_SI25.003. [Date Accessed].

FOR QUESTIONS ABOUT THESE DATA, CONTACT NSIDC@NSIDC.ORG

FOR CURRENT INFORMATION, VISIT https://nsidc.org/data/AE_SI25

National Snow and Ice Data Center

TABLE OF CONTENTS

1 DETAILED DATA DESCRIPTION

1.1 Format

Data are stored in Hierarchical Data Format - Earth Observing System (HDF-EOS) format.

1.2 File and Directory Structure

See the Level-3 25 km Brightness Temperature & Sea Ice Concentration Data Fields document for a list of all HDF-EOS fields. Data files also contain core metadata and product-specific attributes.

1.3 File Naming Convention

This section explains the file naming convention used for this product with examples.

Example file names:

`AMSR_E_L3_SeaIce25km_V15_20080207.hdf`

`AMSR_E_L3_SeaIce25km_X##_yyyymmdd.hdf`

Refer to Table 1 for the values of the file name variables listed above.

Table 1. Variable Values for the File Name

Variable	Description
X	Product Maturity Code (Refer to Table 2 for valid values.)
##	file version number
yyyy	four-digit year
mm	two-digit month
dd	two-digit day
hdf	Hierarchical Data Format (HDF)

Table 2. Variable Values for the Product Maturity Code

Variables	Description
P	Preliminary - refers to non-standard, near-real-time data available from NSIDC. These data are only available for a limited time until the corresponding standard product is ingested at NSIDC.
B	Beta - indicates a developing algorithm with updates anticipated.

Variables	Description
T	Transistional - period between beta and validated where the product is past the beta stage, but not quite ready for validation. This is where the algorithm matures and stabilizes.
V	Validated - products are upgraded to Validated once the algorithm is verified by the algorithm team and validated by the validation teams. Validated products have an associated validation stage. Refer to Table 3 for a description of the stages.

Table 3. Validation Stages

Validation Stage	Description
Stage 1	Product accuracy is estimated using a small number of independent measurements obtained from selected locations, time periods, and ground-truth/field program efforts.
Stage 2	Product accuracy is assessed over a widely distributed set of locations and time periods via several ground-truth and validation efforts.
Stage 3	Product accuracy is assessed, and the uncertainties in the product are well-established via independent measurements made in a systematic and statistically robust way that represents global conditions.

Table 4 provides examples of file name extensions for related files that further describe or supplement data files.

Table 4. Related File Extensions and Descriptions

Extensions for Related Files	Description
.jpg	Browse data
.qa	Quality assurance information
.ph	Product history data
.xml	Metadata files

1.4 File Size

Each daily granule is approximately 20 MB.

1.5 Spatial Coverage

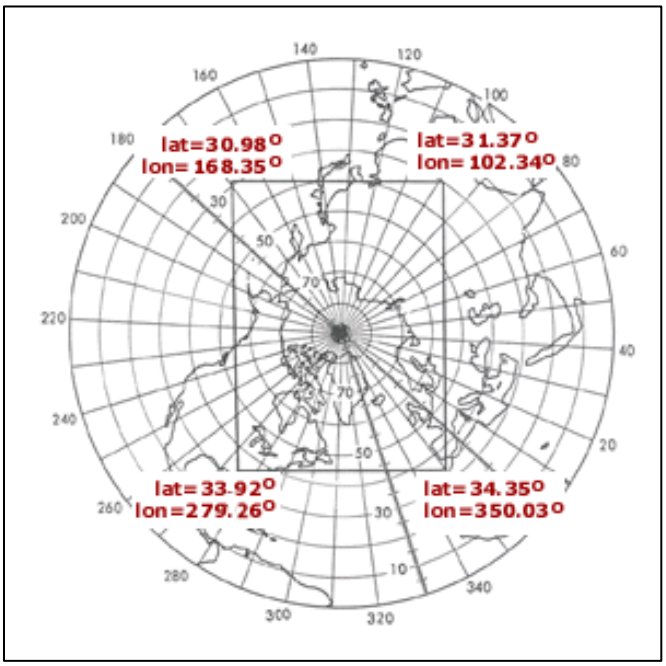

Figure 1. Northern Hemisphere

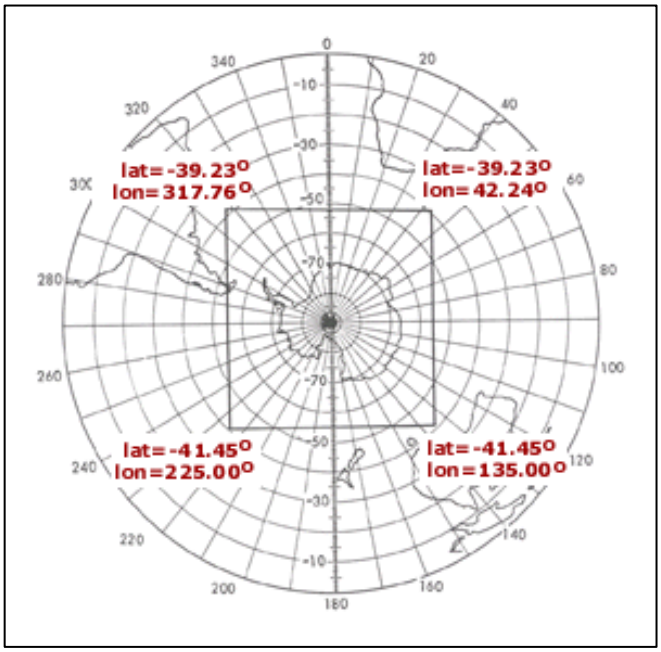

Figure 2. Southern Hemisphere

1.5.1 Spatial Resolution

The spatial resolution of the polar grids is 25 km.

1.6 Projection and Grid Description

1.6.1 Projection

Brightness temperature grids are in a polar stereographic projection, which specifies a projection plane such as the grid tangent to the earth at 70 degrees. The planar grid is designed so that the grid cells at 70 degrees latitude are 25 km by 25 km. For more information on this topic please refer to Pearson (1990) and Snyder (1987).

The polar stereographic projection often assumes that the plane (grid) is tangent to the Earth at the pole. Thus, there is a one-to-one mapping between the Earth's surface and grid with no distortion at the pole. Distortion in the grid increases as the latitude decreases because more of the Earth's surface falls into any given grid cell. At the edge of the northern polar grid distortion reaches 31 percent. The southern polar grid has a maximum distortion of 22 percent. To minimize the distortion, the projection is true at 70 degrees rather than at the poles. This increases the distortion at the poles by three percent and decreases the distortion at the grid boundaries by the same amount. The latitude of 70 degrees was selected so that little or no distortion would occur in the marginal ice zone. Another result of this assumption is that fewer grid cells will be required as the Earth's surface is more accurately represented.

The polar stereographic formula for converting between latitude/longitude and X-Y grid coordinates are taken from Snyder (1982). This projection assumes a Hughes ellipsoid with a radius of 3443.992 nautical mi or 6378.273 km and an eccentricity (e) of 0.081816153 (or e**2 = 0.006693883). The structural metadata (StructMetadata.0) built into the HDF-EOS data file lists the squared eccentricity value rounded to four significant digits (0.006694).

1.6.2 Grid Description

Northern Hemisphere: 304 columns by 448 rows
Southern Hemisphere: 316 columns by 332 rows

The origin of each x, y grid is the pole. The grids' approximate outer boundaries are defined in the following table. Corner points are listed; apply values to the polar grids reading clockwise from upper left. Interim rows define boundary midpoints.

Table 5. North Polar

X (km)	Y (km)	Latitude (deg)	Longitude (deg)	Pixel Location
-3850	5850	30.98	168.35	corner
0	5850	39.43	135.00	midpoint
3750	5850	31.37	102.34	corner
3750	0	56.35	45.00	midpoint
3750	-5350	34.35	350.03	corner
0	-5350	43.28	315.00	midpoint
-3850	-5350	33.92	279.26	corner
-3850	0	55.50	225.00	midpoint

Table 6. South Polar

X (km)	Y (km)	Latitude (deg)	Longitude (deg)	Pixel Location
-3950	4350	-39.23	317.76	corner
0	4350	-51.32	0.00	midpoint
3950	4350	-39.23	42.24	corner
3950	0	-54.66	90.00	midpoint
3950	-3950	-41.45	135.00	corner
0	-3950	-54.66	180.00	midpoint
-3950	-3950	-41.45	225.00	corner
-3950	0	-54.66	270.00	midpoint

For this product, there are files that contain geolocation and pixel-area tools, which provide the same functionality for all polar stereographic passive microwave sea ice data sets at NSIDC. These tools include a FORTRAN routine called locate.for, a latitude/longitude grid, and a pixel-area grid.

The following geocoordinate FORTRAN tools are available via FTP:

locate.for: A FORTRAN routine that allows the user to enter an i,j coordinate and get the corresponding latitude/longitude coordinate, and vice versa.

mapll.for and **mapxy.for**: Subroutines that are associated with the locate.for program. These programs need to be compiled, but are not run explicitly. They are called by locate.for. Thus, the user should compile these programs with locate.for and then use locate to do the conversions.

The latitude/longitude grids are in binary format and are stored as long word integers (4 byte) scaled by 100,000. Each array location (i,j) contains the latitude or longitude value at the center of the corresponding data grid cells. These files are available via FTP.

Table 7. File Variables

Variables	Description
pss	polar stereographic southern projection
psn	polar stereographic northern projection
06, 12, & 25	6 km, 12 km, and 25 km, respectively
lat	latitude grid
lon	longitude grid
area	pixel area

1.7 Temporal Coverage

Data were collected from 01 June 2002 to 4 October 2011.

1.7.1 Temporal Resolution

Brightness temperatures and sea ice concentrations are daily averages, daily ascending averages, and daily descending averages.

1.8 Parameter or Variable

Brightness Temperature (K)
Sea Ice Concentration
Sea Ice Concentration differences between AMSR Bootstrap Algorithm (ABA) and Enhanced NASA Team (NT2)

Refer to the Level-3 25 km Sea Ice Data Fields document for more information regarding the Sea Ice parameters. **Note:** The parameter sea ice temperature was removed from this data product in Version T08.

1.8.1 Parameter Description

This data set contains the following gridded parameters:

- Vertical and horizontal brightness temperatures for the following channels. Separate HDF-EOS fields are provided for ascending, descending, and daily averages.
  - 6.9 GHz
  - 10.7 GHz
  - 18.7 GHz
  - 23.8 GHz
  - 36.5 GHz

    - 89.0 GHz
- Arctic sea ice concentration using the NT2 algorithm. Separate HDF-EOS fields are provided for ascending, descending, and daily averages.
- Antarctic sea ice concentration using the NT2 algorithm. Separate HDF-EOS fields are provided for ascending, descending, and daily averages.
- Arctic and Antarctic sea ice concentration differences between ABA and NT2. Separate HDF-EOS fields are provided for ascending, descending, and daily averages.

2 SOFTWARE AND TOOLS

For tools that work with AMSR-E data, see Tools on the AMSR-E project page.

The NSIDC DataViewer, written in Interactive Data Language (IDL), is also available for use with this data set. The DataViewer is an interactive tool for viewing and displaying satellite images from select NSIDC passive microwave data sets. For more information and access to this tool, refer to the dataviewer.tar.gz section of the Polar Stereographic Data Display Tools web page.

2.1 Quality Assessment

Each HDF-EOS file contains core metadata with Quality Assessment (QA) metadata flags that are set by the Science Investigator-led Processing System (SIPS) at the Global Hydrology and Climate Center (GHCC) prior to delivery to NSIDC. A separate metadata file in XML format is also delivered to NSIDC with the HDF-EOS file; it contains the same information as the core metadata. Three levels of QA are conducted with the AMSR-E Level-2 and -3 products: automatic, operational, and science QA. If a product does not fail QA, it is ready to be used for higher-level processing, browse generation, active science QA, archive, and distribution. If a granule fails QA, SIPS does not send the granule to NSIDC until it is reprocessed. Level-3 products that fail QA are never delivered to NSIDC (Conway 2002).

2.1.1 Automatic QA

Weather filters are employed for the Level-3 sea ice products to eliminate spurious sea ice concentrations over open ocean resulting from varying atmospheric emission. The weather filters are based on threshold values for the spectral gradient ratio and thresholds derived from brightness temperature differences. Sea ice products are checked to see if ice concentration values fall within reasonable limits. These limits are based in part on satellite sea ice climatology developed since the Scanning Multichannel Microwave Radiometer (SMMR) era in 1978.

2.1.2 Operational QA

AMSR-E Level-2A data arriving at GHCC are subject to operational QA prior to processing higher-level products. Operational QA varies by product, but it typically checks for the following criteria in a given file (Conway 2002):

- File is correctly named and sized
- File contains all expected elements
- File is in the expected format
- Required EOS fields of time, latitude, and longitude are present and populated
- Structural metadata is correct and complete
- The file is not a duplicate
- The HDF-EOS version number is provided in the global attributes
- The correct number of input files were available and processed

2.1.3 Science QA

AMSR-E Level-2A data arriving at GHCC are also subject to science QA prior to processing higher-level products. If less than 50 percent of a granule's data is good, the science QA flag is marked suspect when the granule is delivered to NSIDC. In the SIPS environment, the science QA includes checking the maximum and minimum variable values, and percent of missing data and out-of-bounds data per variable value. At the Science Computing Facility (SCF), also at GHCC, science QA involves reviewing the operational QA files, generating browse images, and performing the following additional automated QA procedures (Conway 2002):

- Historical data comparisons
- Detection of errors in geolocation
- Verification of calibration data
- Trends in calibration data
- Detection of large scatter among data points that should be consistent

Geolocation errors are corrected during Level-2A processing to prevent processing anomalies such as extended execution times and large percentages of out-of-bounds data in the products derived from Level-2A data.

The Team Lead SIPS (TLSIPS) developed tools for use at SIPS and SCF for inspecting the data granules. These tools generate a QA browse image in Portable Network Graphics (PNG) format and a QA summary report in text format for each data granule. Each browse file shows Level-2A and Level-2B data. These are forwarded from RSS to GHCC along with associated granule information, where they are converted to HDF raster images prior to delivery to NSIDC.

Refer to AMSR-E Validation Data for information about data used to check the accuracy and precision of AMSR-E observations.

Refer to the AMSR-E Data Quality Web site for more information on quality assessment

3 DATA ACQUISITION AND PROCESSING

3.1 Theory of Measurements

Sea ice concentration products are used to understand the spatial characterization of sea ice cover and to calculate sea ice extent and area for time series analyses and process studies in the Arctic and Antarctic. Passive microwave data are particularly useful for sea ice studies because of the relatively high contrast in emissivities between open water and sea ice. This contrast is frequency-dependent; contrast increases with decreasing channel frequency. In most algorithms, atmospheric effects are assumed constant contributing to uncertainties in the sea ice estimates. The satellite-received radiation, expressed as a Brightness Temperature (T_b), is as follows (Cavalieri and Comiso 2000):

$$T_b = T_{bw}C_w + T_{bi}C_i$$

Where:

T_{bw} = brightness temperature of open water
T_{bi} = brightness temperature of sea ice
C_w = fraction of open water within instrument field-of-view
C_i = fraction of sea ice concentration within the instrument field-of-view

Sea ice concentration (C_I), corresponding to an observed T_b over a sea-ice-covered region (T_b), is derived as follows:

$$C_i = (T_b - T_{bw}) / (T_{bi} - T_{bw})$$

The AMSR-E sea ice concentration products use this equation as a basis for their algorithms, but the channels and methods to derive sea ice concentration are different for each algorithm. Values of brightness temperature of open water, brightness temperature of sea ice include contributions from the intervening atmosphere. Brightness temperature of sea ice varies spatially because of spatial changes in emissivity and temperature of ice, while brightness temperature of open water is constant for open water within the ice pack.

3.2 Data Source

Observations for the 6.9, 10.7, 18.7, 23.8, 36.5, and 89 GHz channels, at native resolutions, from the AMSR-E/Aqua L2A Global Swath Spatially-Resampled Brightness Temperatures are gridded into 25 km grid cells using a drop-in-the-bucket method where the grid cell that contains the center of the observation footprint is given the whole weight of the observation. With this procedure, the

number of observations is always in whole numbers. All valid brightness temperature observations within the extent of the polar grids are binned into grid cells, including land observations.

3.3 Derivation Techniques and Algorithms

3.3.1 Sea Ice Concentration

The 25 km sea ice concentration product is generated using the Enhanced NASA Team (NT2) algorithm described by Markus and Cavalieri (2000) for both the Arctic and the Antarctic. NT2 sea ice concentrations are calculated using the individual Level 2-A swaths rather than using gridded averaged brightness temperatures in order to make the atmospheric corrections on an orbit-by-orbit basis before obtaining daily average ice concentrations. However, previous AE_SI25 versions employed the AMSR Bootstrap Algorithm (ABA) described by Comiso, Cavalieri, and Markus (2003) for the Antarctic. Now the ABA is only used in the sea ice concentration difference field between the ABA and the NT2 (ABA-NT2) for both hemispheres.

The original NASA Team algorithm is based on techniques described in Cavalieri et al. (1984) and Gloersen and Cavalieri (1986). The NT2 algorithm (Markus and Cavalieri 2000) identifies two ice types for both the Arctic and the Antarctic:

Table 8. Polar Ice Types

Arctic	Antarctic
first-year ice	Type A ice consists primarliy of first year ice
multiyear ice	Type B represents sea ice with a heavy snow cover resulting in increased scattering at 37V.

In this algorithm, the primary source of error is attributed to conditions in the surface layer such as surface glaze and layering (Comiso et al. 1997), which can significantly affect the horizontally polarized 18.7 GHz brightness temperature (Matzler et al. 1984) leading to increased PR(18) values and thus is an underestimation of sea ice concentration. The use of the horizontally polarized channels makes it imperative to resolve a third ice type to overcome the difficulty of surface effects on the emissivity of the horizontally polarized component.

Thus, one advantage of using the NT2 algorithm is that it uses the 89 GHz channels because the horizontally polarized 89 GHz data are less affected by surface conditions than the horizontally polarized 18.7 GHz data (Matzler et al. 1984), and the 89 GHz channels have successfully been used in sea ice concentration retrievals under clear atmospheric conditions (Lubin et al. 1998). As a result, this algorithm can identify more complex ice types resulting from surface glaze and layering in the snow cover. The thin-ice bias is also reduced through the use of the third ice type.

The third ice type consists of surface glaze and layering of sea ice with snow cover. This type of ice primarily occurs in the Antarctic.

The Spectral Gradient Ratios (GR) and Polarization Ratios (PRs) are calculated from the observed and modeled brightness temperatures using the following two equations:

The Polarization Equation:

$$\mathrm{PR}(\nu) = \frac{(T_\mathrm{B}(\nu, V) - T_\mathrm{B}(\nu, H))}{(T_\mathrm{B}(\nu, V) + T_\mathrm{B}(\nu, H))}$$

The Spectral Gradient Ratio Equation:

$$\mathrm{GR}(\nu_1, \nu_2, p) = \frac{(T_\mathrm{B}(\nu_1, p) - T_\mathrm{B}(\nu_2, p))}{(T_\mathrm{B}(\nu_1, p) + T_\mathrm{B}(\nu_2, p))}$$

Where:

T_b is the brightness temperature at frequency *v* for the polarized component *p* (vertical (V) or horizontal (H)).

The actual radiance ratios used in the NT2 algorithm are $PR_R(18)$, $PR_R(89)$, GR (89, 18, H-pol), and GR (89, 18, V-pol) where the subscript R refers to a rotation of axes. This rotation is done in the NT PR(18)-GR(37, 18, V-pol) domain, with the axes rotated through an angle, φ, until the ice-type lines (the FY-MY line for the Arctic and the A–B line for the Antarctic) are parallel to the GR axis. The rotated PR is defined by:

$$\mathrm{PR_R}(18) = -\mathrm{GR}(37\mathrm{V}18\mathrm{V})\sin\phi + \mathrm{PR}(18)\cos\phi$$

and is independent of the two ice types. Next, we make use of the difference between two gradient ratios

$$\Delta\mathrm{GR} = \mathrm{GR}(89, 18, \text{H-pol}) - \mathrm{GR}(89, 18, \text{V-pol})$$

to resolve the ambiguity between pixels with true low sea ice concentration and pixels with significant scattering (defined as Ice Type C). Therefore, ΔGR serves as an indicator of the presence of Ice Type C. The higher the value of ΔGR the higher the amount of layering within a pixel. The retrieval of Ice Type C is applied to both, the Arctic and the Antarctic, oceans. Finally, a third parameter is defined to avoid the ambiguity between changes in sea ice concentration and changes in atmospheric conditions, because of the higher sensitivity of the 89-GHz channels to atmospheric variability compared to the lower frequency channels. This third parameter is the

rotated PR(89), $PR_R(89)$, computed from the PR(89)-GR(37V18V) domain analogous to the calculation of $PR_R(18)$ but with a different angle.

The algorithm quantifies atmospheric effects by calculating brightness temperatures for each channel using a forward atmospheric radiative transfer model (Kummerow 1993) that incorporates four surface types: first-year ice, multiyear ice, Type C, and open water. Beginning with version 3, the Southern Hemisphere sea ice concentration algorithm no longer uses the Level-2A land flag and only uses the updated land mask for surface type classification. Thus, the 89 GHz channels together with a forward radiative transfer model provide ice concentrations under all atmospheric conditions. Figure 3 shows the general flow of the algorithm. First brightness temperatures are calculated for the four surface types and all weather conditions, currently 12. The response of the brightness temperatures to different weather conditions is calculated using the atmospheric radiative transfer model. The input data for the model consists of several things such as: the emissivities of the different surface types taken from Table 4-1 in Eppler et al. (1992) with modifications to achieve agreement between modeled and observed ratios, different cloud properties, specifically cloud base, cloud top, and cloud liquid water, taken from Fraser et al. (1975), and average atmospheric temperature and humidity profiles for summer and winter conditions taken from Antarctic research stations. Brightness temperatures are calculated for all possible ice concentration combinations in one percent increments, and the following ratios were calculated for each increment: $PR_R(18)$, $PR_R(89)$, and ΔGR. This creates a prism in which each element within this space contains a vector with the three ratios: $PR_R(18)$, $PR_R(89)$, and ΔGR. The subscript R refers to a rotation of axes in PR-GR space by the angle so that $PR_R(18)$ and $PR_R(89)$ are independent of ice types A and B in the Antarctic, and first-year and multiyear ice for the Arctic. For each pixel, the observed brightness temperatures are used to create a vector with the same ratios. The ice concentration for a pixel is determined where the difference between an observed and a modeled ratio is smallest.

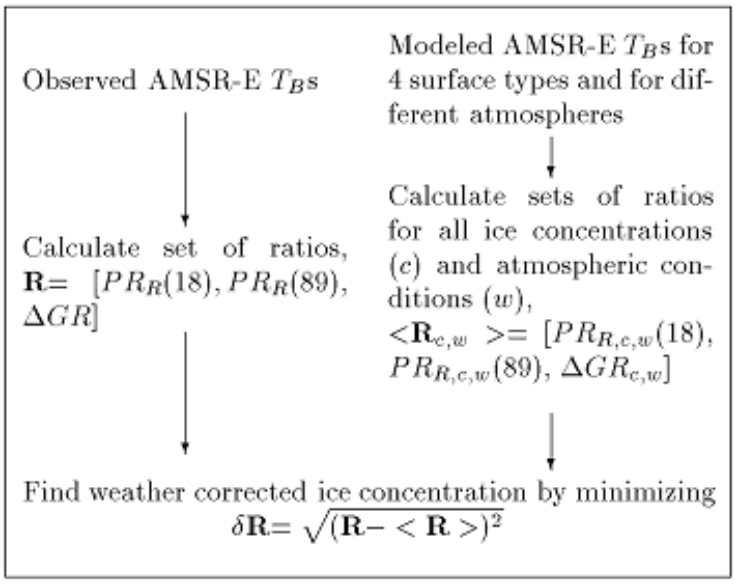

Figure 3. Flow Diagram of Enhanced NASA Team Algorithm

The NT2 algorithm also corrects for the presence of thin ice by using GR(37V19V) and only two ice types. The algorithm eliminates spurious sea ice concentrations over open ocean by employing weather filters previously used for SSM/I (Cavalieri et al. 1995). Ice concentrations for image pixels with GR(37V19V) values greater than 0.05 and GR(2219) values greater than 0.045 are set to zero.

3.3.2 Sea Ice Concentration Difference

The AMSR Bootstrap Algorithm (ABA) (Comiso, Cavalieriand, and Markus 2003) is used in the calculation of sea ice concentration differences between the ABA and the NT2 (ABA-NT2) for both hemispheres. The ABA makes use of the 6.9 GHz data to reduce temperature effects on the 18.7 GHz and 36.5 GHz brightness temperatures, both vertically polarized (called V1937) data provides very similar results to those of the Bootstrap Basic Algorithm (BBA) used in the 12.5 km sea ice product, indicating that errors associated with temperature effects on the latter are relatively minor; however, ABA allows for the calculation of ice temperature, which in itself is an important climate parameter.

3.3.3 Processing Steps

The AMSR-E/Aqua L2A Global Swath Spatially-Resampled Brightness Temperatures are binned into 25 km grid cells using a drop-in-the-bucket method where the grid cell that contains the center of the observation footprint is given the whole weight of the observation. With this procedure, the number of observations is always in whole numbers. All valid brightness temperature observations within the extent of the polar grids are binned into grid cells, including land observations. Figure 2

summarizes the input products and algorithms used to create the gridded 25 km AMSR-E sea ice products.

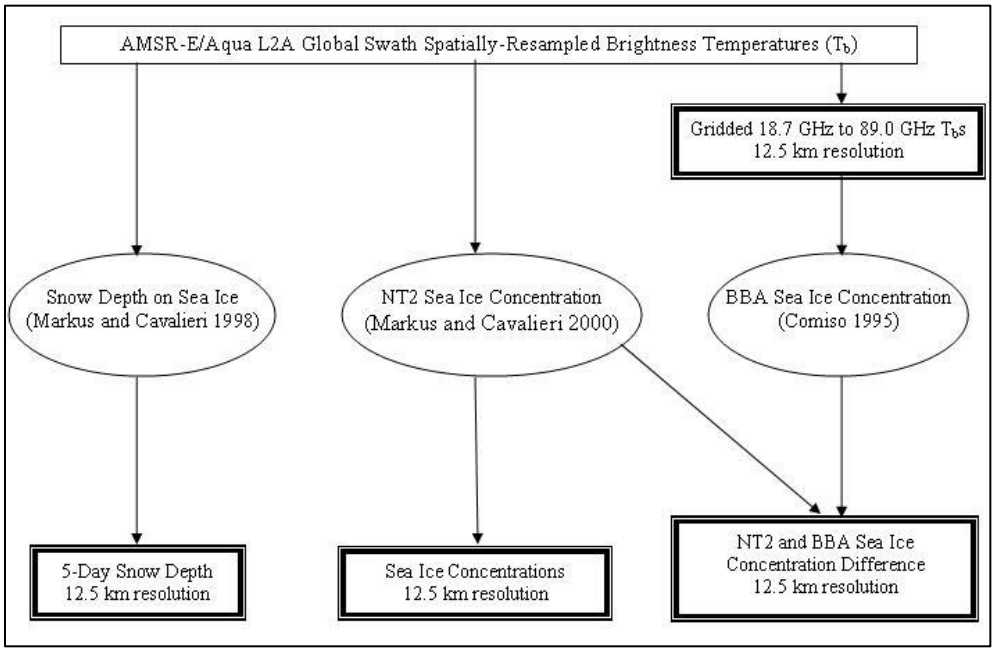

Figure 4. Processing Sequence for AMSR-E 25 km Sea Ice Products

After input Level-2A brightness temperatures are binned into 25 km grid cells, the ascending, descending, and daily data are averaged. Refer to the Data Source section of this guide document for more information. The daily average is not simply an average of ascending and descending orbits, because a given pixel could have, for example, three measurements from ascending orbits and two from descending orbits. Instead, the daily average is of all the observations for that grid cell. For example, if A = ascending and B = descending:

```
((A1 + A2) / 2 + (B1 + B2 + B3) / 3 ) / 2
```

is not equal to:

```
(A1 + A2 + B1 + B2 + B3) / 5
```

However, this biases daytime (ascending) orbits over nighttime (descending).

3.3.3.1 Land Masks

The AMSR-E sea ice product utilizes a 25 km Northern Hemisphere land mask (`amsr_gsfc_25n.hdf`) and a 25 km Southern Hemisphere land mask (`amsr_nic_25s.hdf`). The North land mask is identical to gsfc_25n.msk and was last updated in 1997. The South land mask includes an updated ice shelf definition created by the National Ice Center Science Department in

June 2011 and an updated shoreline developed from ENVISAT and RADARSAT imagery from October 2009 to April 2010.

A 1-byte integer array is included in each HDF file.

`amsr_gsfc_25n.hdf`: 304 columns x 448 rowsValues are 0 (water) and 1 (land).

`amsr_nic_25s.hdf`: 316 columns x 332 rowsValues are 0 (water), 1 (land) and 2 (coast).

3.3.4 Version History

Changes to the Version 3 (V15-stage1) algorithm for these data include:

- Use of the most recent version (Version 3) of the AMSR-E/Aqua L2A Global Swath Spatially-Resampled Brightness Temperatures data as input
- An improved Antarctic land mask
- No longer uses the Level-2A land flag and only uses the updated land mask for surface type classification in the Southern Hemisphere sea ice concentration algorithm
- Inclusion of ISO lineage metadata

Refer to the AMSR-E Data Versions Web page for a summary of changes since the start of mission.

3.3.5 Error Sources

In the sea ice concentration algorithm, the primary source of error is attributed to conditions in the surface layer such as surface glaze and layering (Comiso et al. 1997), which can significantly affect the horizontally polarized 18.7 GHz brightness temperature (Matzler et al. 1984) leading to increased PR(18) values and thus underestimates in ice concentration.

Ashcroft and Wentz (2000) discuss errors in the source Level-2A brightness temperatures that were binned into 25 km grid cells for this sea ice product.

3.4 Sensor or Instrument Description

Please refer to the AMSR-E Instrument Description document.

4 REFERENCES AND RELATED PUBLICATIONS

Cavalieri, D. and J. Comiso. 2000. *Algorithm Theoretical Basis Document for the AMSR-E Sea Ice Algorithm*, Revised December 1. Landover, Maryland USA: Goddard Space Flight Center. (PDF file, 1.4 MB

Cavalieri, D. J., K. M. St. Germain, and C. T. Swift. 1995. Reduction of Weather Effects in the Calculation of Sea Ice Concentration with the DMSP SSM/I. *Journal of Glaciology* 41(139): 455-464.

Cavalieri, D. J., P. Gloersen, and W. J. Campbell. 1984. Determination of Sea Ice Parameters with the NIMBUS-7 SMMR. *Journal of Geophysical Research* 89(D4): 5355-5369.

Comiso, J., D. Cavalieri, and T. Markus. 2003. Sea Ice Concentration, Ice Temperature, and Snow Depth using AMSR-E data. *IEEE Transactions on Geoscience and Remote Sensing* 41(2): 243-252.

Comiso, J. and K. Steffen. 2001. Studies of Antarctic Sea Ice Concentrations from Satellite Data and Their Applications. *Journal of Geophysical Research* 106(C12): 31,361-31,385.

Comiso, J. C., D. J. Cavalieri, C. L. Parkinson, and P. Gloersen. 1997. Passive Microwave Algorithms for Sea Ice Concentration - A Comparison of Two Techniques. *Remote Sensing of the Environment* 60: 357-384.

Comiso, J. C. 1995. *SSM/I Ice Concentrations Using the Bootstrap Algorithm*. NASA RP 1380.

Conway, D. 2002. *Advanced Microwave Scanning Radiometer - EOS Quality Assurance Plan*. Huntsville, AL: Global Hydrology and Climate Center.

Eppler, D. T. and 14 others. 1992. Passive Microwave Signatures of Sea Ice in Microwave Remote Sensing of Ice. *Geophysical Monograph Series* 68: 47-71.

Fraser R. S., N. E.Gaut, E. C. Reifenstein, and H. Sievering. 1975. Interaction Mechanisms Within the Atmosphere Including the Manual of Remote Sensing. *American Society of Photogrammetry* 181-233. Falls Church, VA.

Gloersen P. and D. J. Cavalieri. 1986. Reduction of Weather Effects in the Calculation of Sea Ice Concentration from Microwave Radiances. *Journal of Geophysical Research* 91(C3): 3913-3919.

Gloersen P, W. J. Cambell, D. J. Cavalieri, J. C. Comiso, C. L. Parkinson, and H. J. Zwally. 1992. *Arctic and Antarctic Sea Ice, 1978-1987: Satellite Passive Microwave Observations and Analysis*. Washington, D.C.: National Aeronautics and Space Administration, Special Publication 511.

Kummerow, C. 1993. On the Accuracy of the Eddington Approximation for Radiative Transfer in the Microwave Frequencies. *Journal of Geophysical Research* 98: 2757-2765.

Lubin, D., C. Garrity, R. O. Ramseier, and R. H. Whritner. 1997. Total Sea Ice Concentration Retrieval from the SSM/I 85.5 GHz Channels During the Arctic Summer, *Remote Sensing of Environment* 62: 63-76.

Markus, Thorsten and Donald J. Cavalieri. 2008. [Supplement] AMSR-E Algorithm Theoretical Basis Document: Sea Ice Products. Greenbelt, Maryland USA: Goddard Space Flight Center. (PDF file, 2.10 MB)

Markus, Thorsten and Donald J. Cavalieri. 1998. Snow Depth Distribution over Sea Ice in the Southern Ocean from Satellite Passive Microwave Data. IN: *Antarctic Sea Ice: Physical Processes, Interactions, and Variability*. *Antarctic Research Series* 74:19-39. Washington, DC, USA: American Geophysical Union.

Markus, Thorsten and Donald J. Cavalieri. 2000. An Enhancement of the NASA Team Sea Ice Algorithm. *IEEE Transactions on Geoscience and Remote Sensing* 38: 1387-1398.

Markus, T., D. Cavalieri, and A. Ivanoff. 2011. Algorithm Theoretical Basis Document for the AMSR-E Sea Ice Algorithm, Revised December 2011. Landover, Maryland USA: Goddard Space Flight Center. (PDF file, 528 KB)

Matzler, C., R. O. Ramseier, and E. Svendsen. 1984. Polarization Effects in Sea-ice Signatures. *IEEE Journal of Oceanic Engineering* 9: 333-338.

Pearson, F. 1990. *Map projections: Theory and Applications*. Boca Raton, FL: CRC Press.

Snyder, J.P. 1987. *Map projections - a Working Manual*. U.S. Geological Survey Professional Paper 1395. U.S. Government Printing Office. Washington, D.C.

Snyder, J. P. 1982. *Map Projections Used by the U.S. Geological Survey.* U.S. Geological Survey Bulletin 1532.

4.1 Related Data Collections

Sea Ice Products at NSIDC

This search result lists sea ice data derived from passive microwave sensors and other sources for users who want to compare characteristics of various sea ice products to understand their similarities and differences.

Sea Ice Trends and Climatologies from SMMR and SSM/I-SSMIS

This site provides a suite of value-added products to aid in investigations of the variability and trends of sea ice cover. These products provide users with information about sea ice extent, total ice covered area, ice persistence, monthly climatologies of sea ice concentrations, and ocean masks.

4.2 Related Websites

Sea Ice Remote Sensing at NASA/Goddard Space Flight Center

5 CONTACTS AND ACKNOWLEDGMENTS

Donald J. Cavalieri
Laboratory for Hydrospheric Processes
NASA Goddard Space Flight Center

Josefino Comiso
Laboratory for Hydrospheric Processes
NASA Goddard Space Flight Center

Thorsten Markus
Laboratory for Hydrospheric Processes
NASA Goddard Space Flight Center

6 DOCUMENT INFORMATION

6.1 Publication Date

May 2014

6.2 Date Last Updated

16 June 2021